nature physics

LETTERS

PUBLISHED ONLINE: 21 DECEMBER 2015 | DOI: 10.1038/NPHYS3604

Excitonic luminescence upconversion in a two-dimensional semiconductor

Aaron M. Jones[1†], Hongyi Yu[2†], John R. Schaibley[1], Jiaqiang Yan[3,4], David G. Mandrus[3,4,5], Takashi Taniguchi[6], Kenji Watanabe[6], Hanan Dery[7], Wang Yao[2*] and Xiaodong Xu[1,8*]

Photon upconversion is an elementary light–matter interaction process in which an absorbed photon is re-emitted at higher frequency after extracting energy from the medium. This phenomenon lies at the heart of optical refrigeration in solids[1], where upconversion relies on anti-Stokes processes enabled either by rare-earth impurities[2] or exciton–phonon coupling[3]. Here, we demonstrate a luminescence upconversion process from a negatively charged exciton to a neutral exciton resonance in monolayer WSe_2, producing spontaneous anti-Stokes emission with an energy gain of 30 meV. Polarization-resolved measurements find this process to be valley selective, unique to monolayer semiconductors[4]. Since the charged exciton binding energy[5] closely matches the 31 meV A_1' optical phonon[6–9], we ascribe the spontaneous excitonic anti-Stokes to doubly resonant Raman scattering, where the incident and outgoing photons are in resonance with the charged and neutral excitons, respectively. In addition, we resolve a charged exciton doublet with a 7 meV splitting, probably induced by exchange interactions, and show that anti-Stokes scattering is efficient only when exciting the doublet peak resonant with the phonon, further confirming the excitonic doubly resonant picture.

In solid state systems, spontaneous anti-Stokes emission describes the scattering of low-energy incident photons to higher energy by absorbing energy quanta of lattice oscillations (optical phonons), while Stokes emission refers to the conjugate process of adding phonons to the lattice. The efficiency of these processes can be enhanced by a large optical transition strength in the light–matter interaction, or by realizing doubly resonant conditions, meaning both incident and emitted photons are in resonance with electronic transitions whose energy spacing matches an optical phonon. In semiconductors, doubly resonant Stokes scattering has been observed by applying stress[10], electrical[11], or magnetic fields[12] to tune the band-to-band transitions towards a double resonance, where the excitonic effect realizes an enhancement of the optical transition dipole. However, spontaneous anti-Stokes emission with excitonic double resonance has not been observed. Realizing such a selective enhancement of spontaneous anti-Stokes over Stokes processes implies the appealing possibility of optically cooling semiconductors.

Monolayer semiconductors offer a platform with both strong photon–exciton and phonon–exciton interaction effects[13,14]. The strong Coulomb binding[15–21] leads to large optical transition dipoles of excitons, about one order of magnitude stronger than those in GaAs quantum wells. In particular, monolayer semiconductors possess charged exciton binding energies of the order of tens of meV, which all lie nearly resonant with corresponding optical phonon energies. For instance, in monolayer WSe_2, the negatively charged exciton (X^-) has a binding energy of 30 meV matching the A_1' optical phonon[5–8], that is, X^- plus a phonon is nearly energy degenerate with the neutral exciton (X^o), resulting in a unique excitonic doubly resonant condition[10]. We thus expect that, in addition to electrostatic tunability[5] and exotic valley physics[22–24], monolayer WSe_2 with its large excitonic oscillator strength may offer opportunities to investigate many-body interactions between X^-, X^o and phonons, including X^-–phonon bound states and efficient excitonic anti-Stokes processes with the potential for laser cooling at the monolayer limit.

Here, we report the observation of spontaneous anti-Stokes scattering from the negatively charged exciton to the neutral exciton, enhanced by doubly resonant excitation in monolayer WSe_2, which is simultaneously valley selective and electrically tunable (see Fig. 1a for a device image). We employ low-energy excitation spectroscopy and monitor emission at >5 meV above the excitation energy, referred to hereafter as reverse photoluminescence (PL). After photo-excitation, the resulting luminescence is directed through an adjustable $4f$ spectral filter, which allows the detection of either standard PL (above exciton resonance excitation) or reverse PL, and permits a quantitative comparison between the two (Fig. 1b). The black data of Fig. 1c show the standard PL spectrum near intrinsic doping levels with 1.96 eV excitation. The spectrum consists of X^o and X^- peaks[5].

Remarkably, when exciting 30 meV below the X^o resonance, nearly resonant with X^-, we find significant exciton emission (Fig. 1c, red data). The upconverted luminescence possesses the same line shape and peak energy as X^o obtained in standard PL. Figure 1d presents a log–log plot of upconverted X^o emission versus excitation intensity at 30 K (black data) and 90 K (red data), where we normalize the intensities at 10 μW excitation to facilitate comparison. At both temperatures, we excite 30 meV below the emission peak. As the data all follow the linear relationship indicated by the blue line, we rule out the possibility of nonlinear optical generation of the observed PL upconversion, such as two-photon excitation-induced emission[21,25] and exciton Auger scattering[26,27]. A comparison of the upconverted X^o intensity with standard PL emission under the same excitation conditions reveals a ratio of

[1]Department of Physics, University of Washington, Seattle, Washington 98195, USA. [2]Department of Physics and Center of Theoretical and Computational Physics, University of Hong Kong, Hong Kong, China. [3]Materials Science and Technology Division, Oak Ridge National Laboratory, Oak Ridge, Tennessee 37831, USA. [4]Department of Materials Science and Engineering, University of Tennessee, Knoxville, Tennessee 37996, USA. [5]Department of Physics and Astronomy, University of Tennessee, Knoxville, Tennessee 37996, USA. [6]Advanced Materials Laboratory, National Institute for Materials Science, Tsukuba, Ibaraki 305-0044, Japan. [7]Department of Electrical and Computer Engineering, Department of Physics and Astronomy, University of Rochester, Rochester, New York 14627, USA. [8]Department of Materials Science and Engineering, University of Washington, Seattle, Washington 98195, USA. †These authors contributed equally to this work. *e-mail: wangyao@hku.hk; xuxd@uw.edu

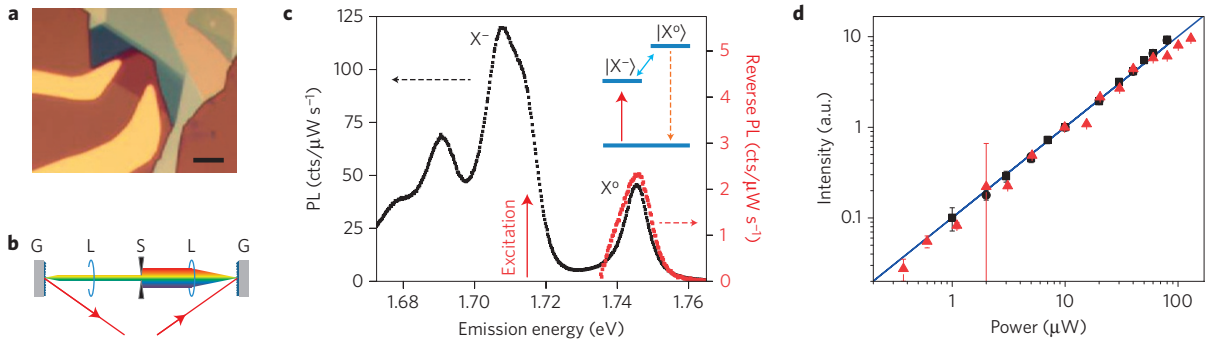

Figure 1 | Upconversion of negatively charged exciton to neutral exciton luminescence. a, Optical micrograph of a device with 5 μm scale bar. **b**, Schematic of the 4*f* spectral filter used in photoluminescence measurements for above- and below-X° excitation (see Methods). **c**, Superposition of photoluminescence spectra for 1.96 eV excitation (black) and 1.715 eV excitation (red), indicated by the red arrow. Inset: upconversion scheme. **d**, Log–log plot of reverse PL intensity as a function of power showing a linear response. Black (red) data correspond to a sample temperature of 30 K (90 K). Intensity has been normalized at 10 μW for clarity, while error bars show the standard deviation of nine points around the PL peak. The blue line is a guide to the eye with a slope of unity.

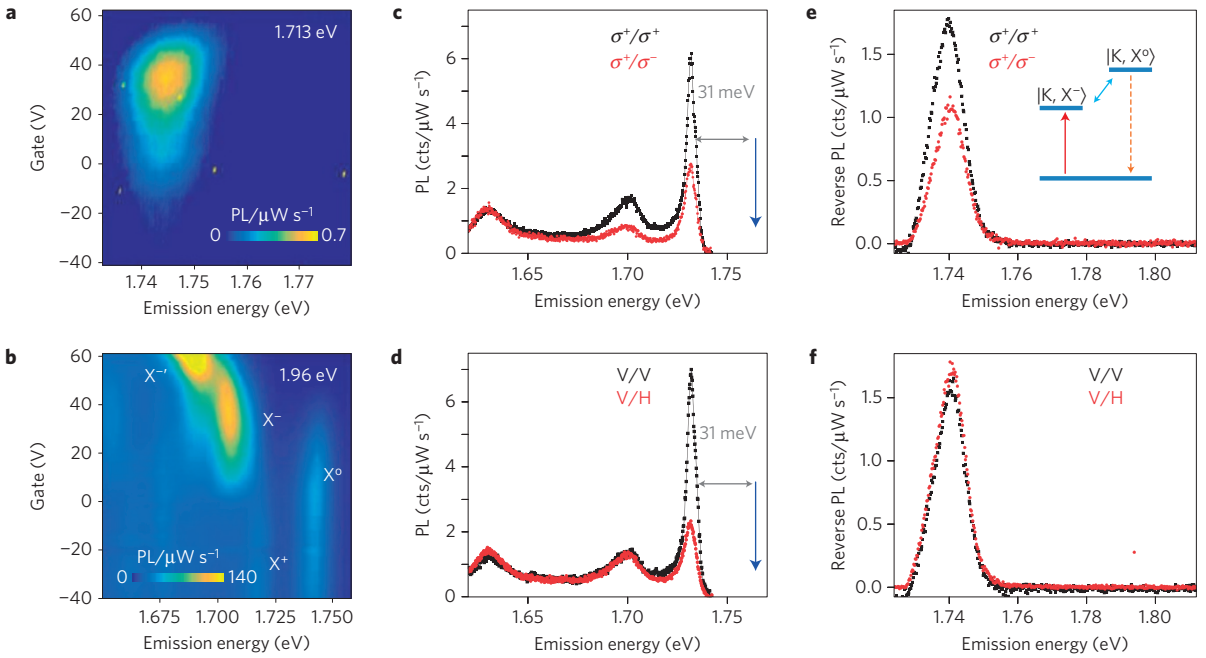

Figure 2 | Gate- and polarization-dependent photoluminescence for excitation above and below the exciton. a,**b**, PL intensity plot as a function of gate and emission energy for an excitation energy of 1.713 eV (**a**) and 1.96 eV (**b**). **c**,**d**, Polarization-resolved PL spectra with an excitation energy one optical phonon (31 meV) above the neutral exciton for circular (σ^+) (**c**) and linear (V) (**d**) polarized excitation. Blue arrows indicate the laser excitation position. **e**,**f**, Polarization-resolved reverse PL spectra with 1.714 eV excitation (30 meV below neutral exciton), for circularly (**e**) and linearly (**f**) polarized excitation/detection. Inset in **e** illustrates the valley-selective spontaneous anti-Stokes process. The solid red arrow denotes photon excitation, the blue arrow doubly resonant phonon scattering, and the dashed orange arrow spontaneous photon emission.

about 5%, a notable contrast given that 30 meV at 30 K represents an energy gain $>10k_BT$.

What is the origin of the upconversion from the X^- resonance to X^o? One possibility is that an exciton–phonon replica of X^o exists near the X^- resonance, since both A_1' and E′ phonons may produce replicas about 30 meV from the zero-phonon peak[8]. We rule out such an explanation through two experiments. First, we perform a gate-dependent study of reverse PL with excitation 30 meV below X^o (Fig. 2a). The upconverted emission at X^o reaches peak intensity at a gate voltage $V_g \approx 35$ V, where electron doping leads to maximum X^- state emission in conventional PL, and lies outside the doping range where X^o PL is appreciable (see Fig. 2b). In addition, the reverse PL intensity plot in Fig. 2a does not show resonant luminescence upconversion from X^+ in the hole-doping regime. Were the high-energy PL simply due to upconversion of an exciton–phonon replica near X^-, its behaviour would be symmetric with respect to gate voltage.

Second, we examine polarization-resolved PL for excitation 31 meV above the X^o resonance—that is, resonant Stokes scattering. Figure 2c,d clearly demonstrates that the emission at X^o preserves both the circular and linear polarization of the excitation laser, showing that the involved phonon scattering preserves both the valley polarization and coherence, consistent with recent photoluminescence excitation[28] (PLE) and Raman[8] spectroscopy measurements. From the complete absence of linearly polarized PL near the X^- resonance (Fig. 2d), we can rule out the possibility of an X^o phonon replica near X^-, as it would inherit the linearly polarized emission of X^o.

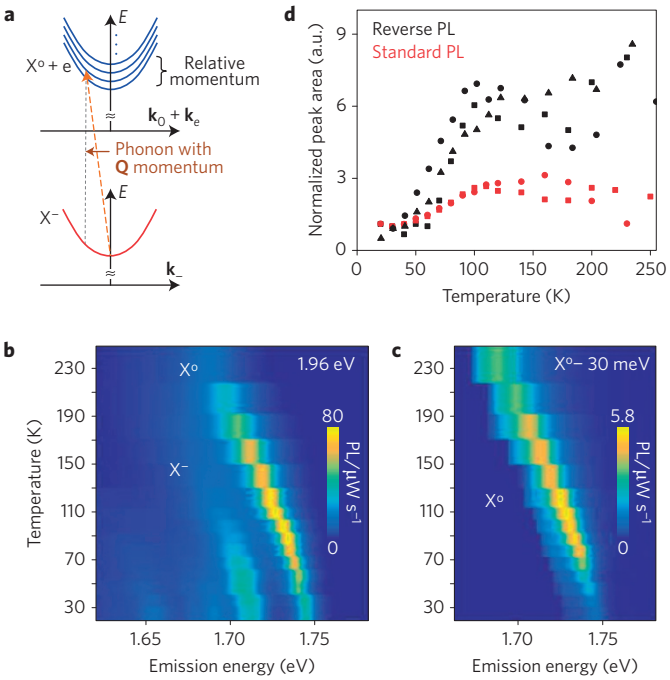

Figure 3 | Doubly resonant anti-Stokes and temperature-dependent PL. **a**, Schematic of the negatively charged and neutral exciton energy level diagram. The red curve is the charged exciton dispersion with its centre-of-mass momentum $\mathbf{k}_-$. The blue curves are the dispersions of the unbound exciton–electron pair with their centre-of-mass momentum $\mathbf{k}_0 + \mathbf{k}_e$, different curves correspond to different relative momenta so they form an energy continuum. By absorbing a phonon with momentum $\mathbf{Q}$, the charged exciton can be converted into an unbound exciton–electron pair (dashed arrow). **b**,**c**, Temperature-dependent PL intensity plot for excitation at 1.96 eV (**b**) and 30 meV (**c**) below peak emission. **d**, Integrated X° peak intensity versus temperature, extracted from three different samples, normalized to the intensity at 30 K.

Further, our polarization-resolved reverse PL also shows that the luminescence upconversion conserves valley polarization, but not valley coherence. As seen in Fig. 2e, circularly polarized excitation of X^- creates co-circularly polarized X° emission, but linearly polarized excitation yields unpolarized anti-Stokes X° emission (Fig. 2f and Supplementary Fig. 1). This contrast between pronounced circular polarization and an absence of linear polarization in the upconverted X° luminescence mirrors the behaviour of X^- PL (ref. 5), implying the luminescence upconversion originates from X^-.

In light of the fact that the 30 meV separation between X° and X^- coincides with the A_1' phonon (31 meV), we attribute the observed luminescence upconversion to an excitonic doubly resonant anti-Stokes process. The anti-Stokes scattering here involves a single phonon resonant with the separation of X^- and X° ground states, in contrast with the exciton excited-state multi-phonon Raman scattering discussed in ref. 28, which involves multiple detuned intermediate states and does not result in upconversion. We note that, although the E′ phonon also lies at 31 meV, its role would be negligible in upconversion. The polarization-resolved measurements already presented show a preservation of valley polarization for excitation both above and below X°, consistent with the polarization properties of the A_1' phonon[8]. In contrast, Raman from the E′ mode is cross-polarized[8] and unpolarized[29] for circularly and linearly polarized excitation, respectively. Furthermore, the symmetry of the electronic states within the K valleys dictates a stronger interaction with the out-of-plane A_1' phonon than with the in-plane E′ mode[14,30] (see Supplementary Methods I).

In the doubly resonant anti-Stokes process, the photon resonantly excites X^-, which is converted into X° plus an unbound electron by absorbing an A_1' phonon from the environment (Fig. 3a). Spontaneous emission from X° then produces the upconverted luminescence. We have found that the transfer of population from X^- to X° is well described by Fermi's golden rule (see Supplementary Methods II and III), where the conversion rate is proportional to the A_1' phonon population and can reach 0.01 ps^{-1} at a temperature of ≈100 K. This model explains both the polarization-resolved PL and reverse PL measurements already discussed, where the conservation of circular (that is, valley) but not linear polarization within the upconverted X° is a straightforward consequence of inheriting the X^- properties[5].

The upconversion seen here implies efficient population transfer between X^- and X° mediated by resonant phonons, where the absorption/emission of a phonon resonantly induces X^- discharging/X° charging. Correspondingly, higher lattice temperatures should increase the ratio between the upconversion and the downconversion rates of X^- and X°, and we expect a temperature increase to raise the intensity ratio between X° and X^- in standard PL. Our temperature-dependent measurements show behaviour consistent with this picture. Figure 3b,c presents temperature-dependent standard and reverse PL maps, respectively, over a temperature range of 20–250 K. In standard PL measurements, we fix the excitation energy at 1.96 eV, while for reverse PL we maintain an excitation energy 30 meV below the energy of peak X° emission for each temperature. Across three samples we find a consistent intensity increase of both the standard and reverse X° PL up to 100 K (Fig. 3d), a consequence of the upconversion rate increasing with the phonon population. Above 100 K, the growth halts as decreasing trion absorption and X° radiative decay rates counteract the increasing phonon population. Detailed analysis shows the temperature-dependent behaviour of the reverse PL to be in agreement with calculations of upconversion within a phonon-induced discharging model (see discussion in Supplementary Methods V).

Careful examination of the X^- spectrum further reveals a doublet structure. As shown in Fig. 4a, this X^- doublet can be fit with two Gaussians, which we label as states $X^-_{|2\rangle}$ (high energy) and $X^-_{|1\rangle}$ (low energy), shown by the blue lines (see Supplementary Fig. 2 for an obvious doublet in boron-nitride-supported WSe_2,). Through reverse PLE measurements, in which we monitor X° emission while varying the excitation energy from 1.691 eV to 1.722 eV (red detunings of 23–55 meV from X°), we find that the higher energy peak, $X^-_{|2\rangle}$, dominates the upconversion. Figure 4b gives the reverse PLE intensity plot as a function of excitation and luminescence energy, where the anti-Stokes luminescence reaches a maximum for an excitation energy of 1.716 eV. We extract the PLE spectrum by taking a line cut at peak X° intensity and superpose it with the X^- doublet (red squares in Fig. 4a). Clearly, the spectrum peak coincides with $X^-_{|2\rangle}$. For this particular sample, we find a low-energy tail extending over $X^-_{|1\rangle}$, although other samples reveal a PLE spectrum more localized to the $X^-_{|2\rangle}$ state (Supplementary Fig. 3). This correspondence supports the attribution of the upconversion to doubly resonant excitonic anti-Stokes, since the phonon energy matches the X° and $X^-_{|2\rangle}$ energy separation, while $X^-_{|1\rangle}$ lies at a detuning of 7 meV, rendering phonon scattering inefficient. We also find within the X^- doublet a strong excitation wavelength and polarization dependence (see Supplementary Fig. 4). For instance, $X^-_{|2\rangle}$ exhibits a larger degree of circular polarization than $X^-_{|1\rangle}$ in standard PL (Fig. 4c and Supplementary Fig. 4a).

From the above experimental facts, we attribute the observed doublet to X^- fine structure induced by the diagonal exchange interaction between the electron and hole constituents (green double arrows in Fig. 4d). In WSe_2, the negatively charged exciton has two exchange-split branches[31,32], with circularly polarized

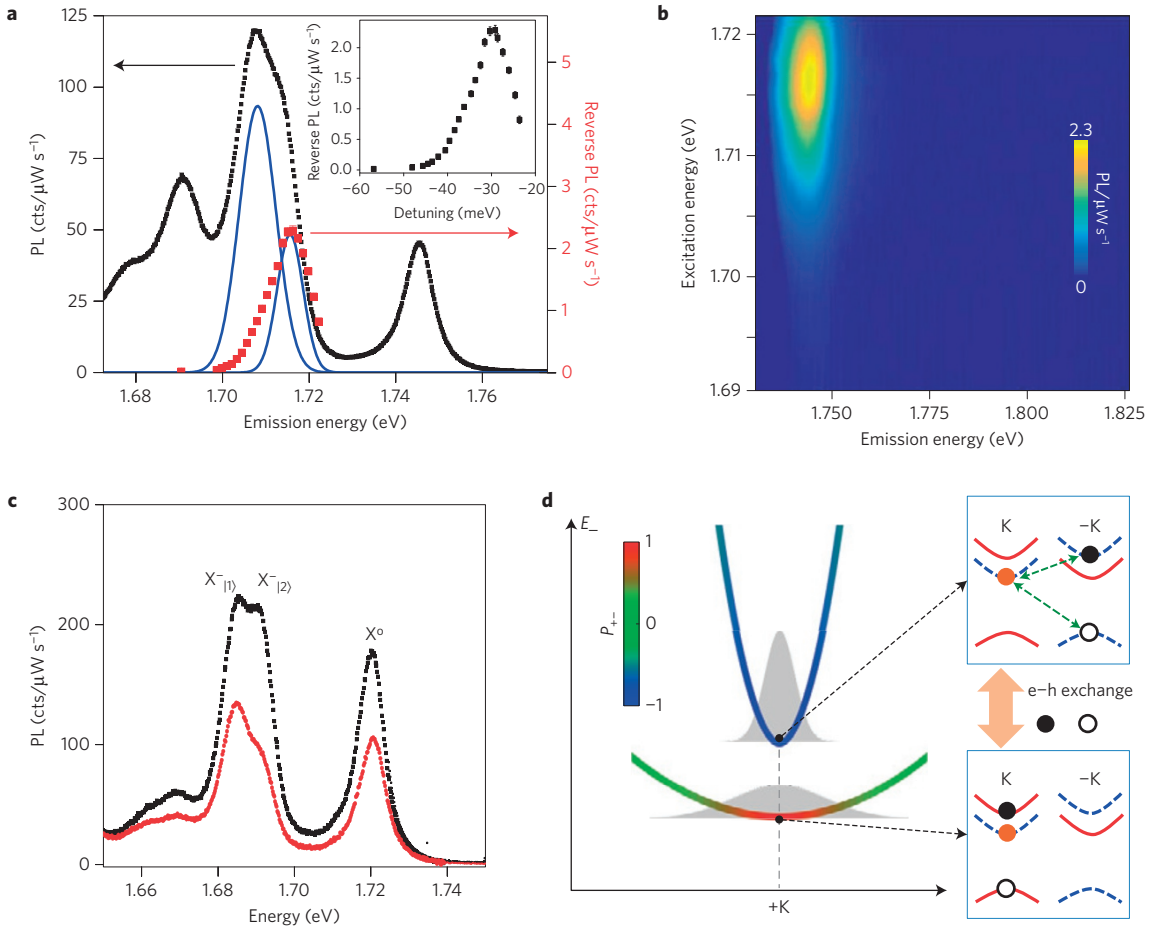

Figure 4 | Negatively charged exciton fine structure and its role in anti-Stokes. a, Comparison of reverse PLE intensity (red) and conventional PL spectrum (black), with a bi-Gaussian fit to the charged exciton X^- peak doublet (blue). Inset: Reverse PLE intensity versus laser detuning, with error bars showing the standard deviation of nine points around the PL peak. **b**, Reverse PLE intensity plot as a function of excitation and emission energy. **c**, Polarization-resolved PL spectra with σ^+ polarized excitation at 1.96 eV. Black and red curves are co-circular and cross circular detection, respectively. **d**, Right: Top and bottom cartoons show the inter-valley and intra-valley X^-. The diagonal exchange interaction present for the inter-valley X^- (green double arrows) lifts the energy degeneracy with intra-valley configurations. Moreover, the inter- and intra-valley X^- are coupled by the off-diagonal electron–hole exchange interaction (thick orange double arrow). These exchange effects lead to the two split dispersions of X^- shown on the left, where the degree of circular polarization of photon emission (denoted by colour) decreases with momentum. Because of the steeper dispersion of the higher-energy branch, the same thermal broadening in energy corresponds to a narrower distribution in momentum (depicted by the shaded area), and hence a larger degree of polarization than the lower-energy X^- branch.

emission at the dispersion minima and linearly polarized emission at large kinetic energies (Fig. 4d). The off-diagonal electron–hole exchange interaction at finite velocity (thick orange double arrow in Fig. 4d) is largely responsible for depolarization of both neutral and charged excitons[5]. The steeper dispersion of the upper branch causes a narrower distribution of the velocities at a given temperature, leading to less depolarization of the luminescence compared to the lower X^- branch (Fig. 4d). This is consistent with our PL measurements showing larger circular polarization for $X^-_{|2\rangle}$ than $X^-_{|1\rangle}$. Further, more efficient formation of $X^-_{|2\rangle}$ compared to $X^-_{|1\rangle}$ also contributes to its larger PL polarization[32]. Our measurements across 14 samples find a mean X^- peak splitting of 6.9 ± 0.5 meV, with little temperature dependence (see Supplementary Fig. 5), consistent with theoretical estimations[31–33]. Such a large splitting reveals the exchange interaction in monolayer WSe_2 to be an order of magnitude stronger than in GaAs systems, a direct consequence of strong Coulomb interactions within this 2D semiconductor.

We note that when the excitation laser energy is significantly higher than the X^0 resonance, $X^-_{|1\rangle}$ and $X^-_{|2\rangle}$ can have various formation channels, including multiple phonon emission[28], while the excess laser energy facilitates a dynamical equilibration between X^0, $X^-_{|1\rangle}$ and $X^-_{|2\rangle}$. Thus, all three constituents appear in the PL spectrum when exciting at higher energy. If, on the other hand, the laser resonantly excites X^0, the most efficient X^- formation channel is the single-phonon emission process discussed above. Here, alignment of the X^0–$X^-_{|2\rangle}$ energy separation with the A_1' phonon energy favours the formation of $X^-_{|2\rangle}$ instead of $X^-_{|1\rangle}$. This is consistent with the observed behaviour of both luminescence upconversion (seen in reverse PL) and downconversion (for example, standard PL under resonant X^0 excitation) by single-phonon absorption and emission, respectively.

In summary, our report of luminescence upconversion from the negatively charged to neutral exciton resonances with valley selectivity and electrical control stems from the doubly resonant condition of Raman scattering, which is selectively fulfilled in anti-Stokes, but not Stokes, processes. Since the degeneracy between a Raman active optical phonon energy and the charged exciton binding energy exists in other monolayer transitional metal dichalcogenides (for example, monolayer $MoSe_2$), the conditions for doubly resonant anti-Stokes are likewise satisfied. We remark that the observation of excitonic upconversion enhanced by doubly resonant Raman scattering could be general within these 2D

semiconductors, and may imply a new cooling channel for 2D semiconductors. Our results reveal strong interactions between ground-state neutral and charged excitons mediated by resonant phonons, a new aspect of 2D exciton physics, which will impact our fundamental understanding of existing and future experiments on valley excitons in 2D semiconductors.

Methods

Methods and any associated references are available in the online version of the paper.

Received 10 September 2015; accepted 13 November 2015; published online 21 December 2015

References

1. Pringsheim, P. Bemerkungen über den Unterschied von Lumineszenz-und Temperaturstrahlung. *Z. Phys.* **57,** 739–746 (1929).
2. Epstein, R. I. *et al.* Observation of laser-induced fluorescent cooling of a solid. *Nature* **377,** 500–503 (1995).
3. Zhang, J., Li, D., Chen, R. & Xiong, Q. Laser cooling of a semiconductor by 40 kelvin. *Nature* **493,** 504–508 (2013).
4. Xiao, D., Liu, G.-B., Feng, W., Xu, X. & Yao, W. Coupled spin and valley physics in monolayers of MoS_2 and other group-VI dichalcogenides. *Phys. Rev. Lett.* **108,** 196802 (2012).
5. Jones, A. M. *et al.* Optical generation of excitonic valley coherence in monolayer WSe_2. *Nature Nanotech.* **8,** 634–638 (2013).
6. Tonndorf, P. *et al.* Photoluminescence emission and Raman response of monolayer MoS_2, $MoSe_2$, and WSe_2. *Opt. Express* **21,** 4908–4916 (2013).
7. Sahin, H. *et al.* Anomalous Raman spectra and thickness-dependent electronic properties of WSe_2. *Phys. Rev. B* **87,** 165409 (2013).
8. Chen, S.-Y., Zheng, C., Fuhrer, M. S. & Yan, J. Helicity resolved Raman scattering of MoS_2, $MoSe_2$, WS_2 and WSe_2 atomic layers. *Nano Lett.* **15,** 2526–2532 (2015).
9. Zhang, X. *et al.* Phonon and Raman scattering of two-dimensional transition metal dichalcogenides from monolayer, multilayer to bulk material. *Chem. Soc. Rev.* **44,** 2757–2785 (2015).
10. Cerdeira, F., Anastassakis, E., Kauschke, W. & Cardona, M. Stress-induced doubly resonant Raman scattering in GaAs. *Phys. Rev. Lett.* **57,** 3209–3212 (1986).
11. Agulló-Rueda, F., Mendez, E. & Hong, J. Doubly resonant Raman scattering induced by an electric field. *Phys. Rev. B* **38,** 12720–12723 (1988).
12. Gubarev, S. I., Ruf, T. & Cardona, M. Doubly resonant Raman scattering in the semimagnetic semiconductor $Cd_{0.95}Mn_{0.05}Te$. *Phys. Rev. B* **43,** 1551–1554 (1991).
13. Kaasbjerg, K., Thygesen, K. S. & Jacobsen, K. W. Phonon-limited mobility in n-type single-layer MoS_2 from first principles. *Phys. Rev. B* **85,** 115317 (2012).
14. Carvalho, B. R., Malard, L. M., Alves, J. M., Fantini, C. & Pimenta, M. A. Symmetry-dependent exciton-phonon coupling in 2D and bulk MoS_2 observed by resonance Raman scattering. *Phys. Rev. Lett.* **114,** 136403 (2015).
15. Qiu, D. Y., Da Jornada, F. H. & Louie, S. G. Optical spectrum of MoS_2: Many-body effects and diversity of exciton states. *Phys. Rev. Lett.* **111,** 216805 (2013).
16. Ye, Z. *et al.* Probing excitonic dark states in single-layer tungsten disulphide. *Nature* **5,** 214–218 (2014).
17. Chernikov, A. *et al.* Exciton binding energy and nonhydrogenic Rydberg series in monolayer WS_2. *Phys. Rev. Lett.* **113,** 076802 (2014).
18. Zhang, C., Johnson, A., Hsu, C. L., Li, L. J. & Shih, C. K. Direct imaging of band profile in single layer MoS_2 on graphite: Quasiparticle energy gap, metallic edge states, and edge band bending. *Nano Lett.* **14,** 2443–2447 (2014).
19. He, K. *et al.* Tightly bound excitons in monolayer WSe_2. *Phys. Rev. Lett.* **113,** 026803 (2014).
20. Ugeda, M. M. *et al.* Giant bandgap renormalization and excitonic effects in a monolayer transition metal dichalcogenide semiconductor. *Nature Mater.* **13,** 1091–1095 (2014).
21. Wang, G. *et al.* Giant enhancement of the optical second-harmonic emission of WSe_2 monolayers by laser excitation at exciton resonances. *Phys. Rev. Lett.* **114,** 097403 (2015).
22. Mak, K. F., He, K., Shan, J. & Heinz, T. F. Control of valley polarization in monolayer MoS_2 by optical helicity. *Nature Nanotech.* **7,** 494–498 (2012).
23. Cao, T. *et al.* Valley-selective circular dichroism of monolayer molybdenum disulphide. *Nature Commun.* **3,** 887 (2012).
24. Zeng, H., Dai, J., Yao, W., Xiao, D. & Cui, X. Valley polarization in MoS_2 monolayers by optical pumping. *Nature Nanotech.* **7,** 490–493 (2012).
25. Seyler, K. L. *et al.* Electrical control of second-harmonic generation in a WSe_2 monolayer transistor. *Nature Nanotech.* **10,** 407–411 (2015).
26. Kumar, N. *et al.* Exciton–exciton annihilation in $MoSe_2$ monolayers. *Phys. Rev. B* **89,** 125427 (2014).
27. Mouri, S. *et al.* Nonlinear photoluminescence in atomically thin layered WSe_2 arising from diffusion-assisted exciton–exciton annihilation. *Phys. Rev. B* **90,** 155449 (2014).
28. Wang, G. *et al.* Double resonant Raman scattering and valley coherence generation in monolayer WSe_2. *Phys. Rev .Lett.* **115,** 117401 (2015).
29. Zhao, W. *et al.* Lattice dynamics in mono- and few-layer sheets of WS_2 and WSe_2. *Nanoscale* **5,** 9677–9683 (2013).
30. Chakraborty, B. *et al.* Symmetry-dependent phonon renormalization in monolayer MoS_2 transistor. *Phys. Rev. B* **85,** 161403(R) (2012).
31. Yu, H., Cui, X., Xu, X. & Yao, W. Valley excitons in two-dimensional semiconductors. *Natl Sci. Rev.* **2,** 57–70 (2014).
32. Aivazian, G. *et al.* Magnetic control of valley pseudospin in monolayer WSe_2. *Nature Phys.* **11,** 148–152 (2015).
33. Yu, H., Liu, G.-B., Gong, P., Xu, X. & Yao, W. Dirac cones and Dirac saddle points of bright excitons in monolayer transition metal dichalcogenides. *Nature Commun.* **5,** 3876 (2014).

Acknowledgements

We thank R. Merlin and D. Cobden for helpful discussions. This work is mainly supported by the Department of Energy, Basic Energy Sciences, Materials Sciences and Engineering Division (DE-SC0008145 and SC0012509). H.Y. and W.Y. are supported by the Croucher Foundation (Croucher Innovation Award), and the RGC and UGC of Hong Kong (HKU17305914P, HKU9/CRF/13G, AoE/P-04/08). J.Y. and D.G.M. are supported by US DoE, BES, Materials Sciences and Engineering Division. H.D. is supported by Department of Energy under Contract No. DE-SC0014349 and National Science Foundation under Contract No. DMR-1503601. X.X. acknowledges a Cottrell Scholar Award, support from the State of Washington-funded Clean Energy Institute, and support from the Boeing Distinguished Professorship in Physics. Device fabrication was performed at the University of Washington Microfabrication Facility and NSF-funded Nanotech User Facility.

Author contributions

X.X. and W.Y. conceived and supervised the experiments; A.M.J. fabricated the devices and performed measurements, assisted by J.R.S.; A.M.J., H.Y., X.X., W.Y. analysed the data with discussion from H.D.; J.Y. and D.G.M. provided and characterized the bulk WSe_2; T.T. and K.W. provided BN crystals; A.M.J., X.X., W.Y., H.Y. wrote the paper. All authors discussed the results.

Additional information

Supplementary information is available in the online version of the paper. Reprints and permissions information is available online at www.nature.com/reprints. Correspondence and requests for materials should be addressed to W.Y. or X.X.

Competing financial interests

The authors declare no competing financial interests.

Methods

Monolayer WSe_2 crystals are first obtained by mechanical exfoliation of bulk WSe_2 crystals onto a SiO_2/Si wafer and visually identified in an optical microscope, after which electrical contacts are patterned using standard lithographic techniques. To spectrally resolve individual excitonic states, we perform measurements at cryogenic temperatures (30 K), unless otherwise noted. For standard PL measurements, we use a 633 nm HeNe laser as the excitation source. For low-energy excitation, we employ the output of an ultra-narrow linewidth MSquared SolsTiS laser, with a tunable wavelength range of 690–950 nm.

Spectral filtering for the reverse PL measurements is accomplished in three stages. First, a long-pass filter eliminates the high-energy tail of the SolsTiS excitation beam. Second, a 750 nm short-pass filter on the detection side removes remnant components at wavelengths well above the X^o resonance. Third, a 4*f* spectral filter provides a continuously tunable short- or long-pass spectral filter (see Fig. 1b). By placing two gratings (G) at the outside conjugate focal planes of two lenses (L), the beam is focused at the central focal plane, with the spectral distribution mapped into a spatial separation. Placement of an adjustable slit (S) at the central focal plane allows tunable pass-band selection.